Layer-by-Layer Thinning of MoS_2 by Plasma

Yulu Liu,[†,∥] Haiyan Nan,[†,∥] Xing Wu,[‡] Wei Pan,[§] Wenhui Wang,[†] Jing Bai,[†] Weiwei Zhao,[⊥] Litao Sun,[‡] Xinran Wang,[§] and Zhenhua Ni[†,*]

[†]Department of Physics, Southeast University, SEU Research Center of Converging Technology, Nanjing 211189, China, [‡]SEU-FEI Nano-Pico Center, Key Laboratory of MEMS of Ministry of Education, School of Electrical Science and Engineering, Southeast University, Nanjing 210096, China, [§]National Laboratory of Microstructures, School of Electronic Science and Engineering, Nanjing University, Nanjing 210093, China, and [⊥]Jiangsu Key Laboratory for Design and Fabrication of Micro-Nano Biomedical Instruments, School of Mechanical Engineering, Southeast University, Nanjing 211189, China. [∥]These authors contributed equally to this work.

ABSTRACT The electronic structures of two-dimensional materials are strongly dependent on their thicknesses; for example, there is an indirect to direct band gap transition from multilayer to single-layer MoS_2. A simple, efficient, and nondestructive way to control the thickness of MoS_2 is highly desirable for the study of thickness-dependent properties as well as for applications. Here, we present layer-by-layer thinning of MoS_2 nanosheets down to monolayer by using Ar^+ plasma. Atomic force microscopy, high-resolution transmission electron microscopy, optical contrast, Raman, and photoluminescence spectra suggest that the top layer MoS_2 is totally removed by plasma while the bottom layer remains almost unaffected. The evolution of Raman and photoluminescence spectra of MoS_2 with thickness change is also investigated. Finally, we demonstrate that this method can be used to prepare two-dimensional heterostructures with periodical single-layer and bilayer MoS_2. The plasma thinning of MoS_2 is very reliable (with almost 100% success rate), can be easily scaled up, and is compatible with standard semiconductor process to generate heterostructures/patterns at nanometer scale, which may bring out interesting properties and new physics.

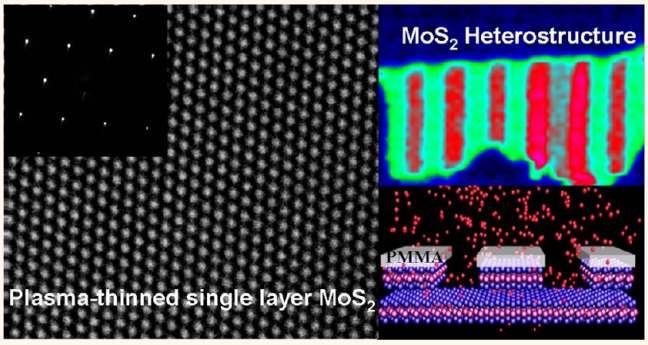

KEYWORDS: MoS_2 · plasma-induced thinning · Raman · photoluminescence · contrast

Two-dimensional layered materials have received great attention since the first experimental discovery of graphene in 2004.[1−4] Among them, single-layer and multilayer MoS_2 have exhibited interesting properties compared to its bulk form[5] and other two-dimensional materials. MoS_2 devices exhibit a room-temperature current on/off ratio of $\sim 1 \times 10^8$ (due to the large intrinsic band gap) and carrier mobility up to 200 $cm^2\ V^{-1}\ s^{-1}$.[6−8] An indirect to direct band gap transition from multilayer to single-layer MoS_2 was also reported, which results in great enhancement of photoluminescence (PL).[9,10] More interesting phenomena were presented; for example, electronic structure enables valley polarization,[11−13] robust mechanical properties, and strain tunable band gap.[14−16] The fabrication of large-scale MoS_2 film using chemical vapor deposition[17−19] and a large quantity of MoS_2 nanosheets using solution-based chemical exfoliation[20,21] also represents important steps for its wafer-scale application in electronic devices and flexible and transparent optoelectronics.

The electronic properties of two-dimensional layered materials are strongly dependent on their thicknesses.[4,22] Single-layer MoS_2 has a direct band gap of ~1.9 eV, which makes it promising for application in optoelectronic devices, such as photodetectors,[23,24] photovoltaics,[16] and light emitters.[25] In addition, multilayer MoS_2 may also provide different and interesting properties, similar to what happened in multilayer graphene.[22,26,27] The thickness-modulated optical energy gap of MoS_2 is desirable for phototransistors.[24] Electronic devices based on multilayer MoS_2 were also reported.[7,28,29] Therefore, a simple and efficient approach to control the thickness of MoS_2 is highly desirable. It will also enable the study of thickness-dependent properties of MoS_2. Recently, Castellanos-Gomez *et al.* presented an exciting work using a

* Address correspondence to zhni@seu.edu.cn.

Received for review February 6, 2013 and accepted April 2, 2013.

Published online April 02, 2013
10.1021/nn400644t

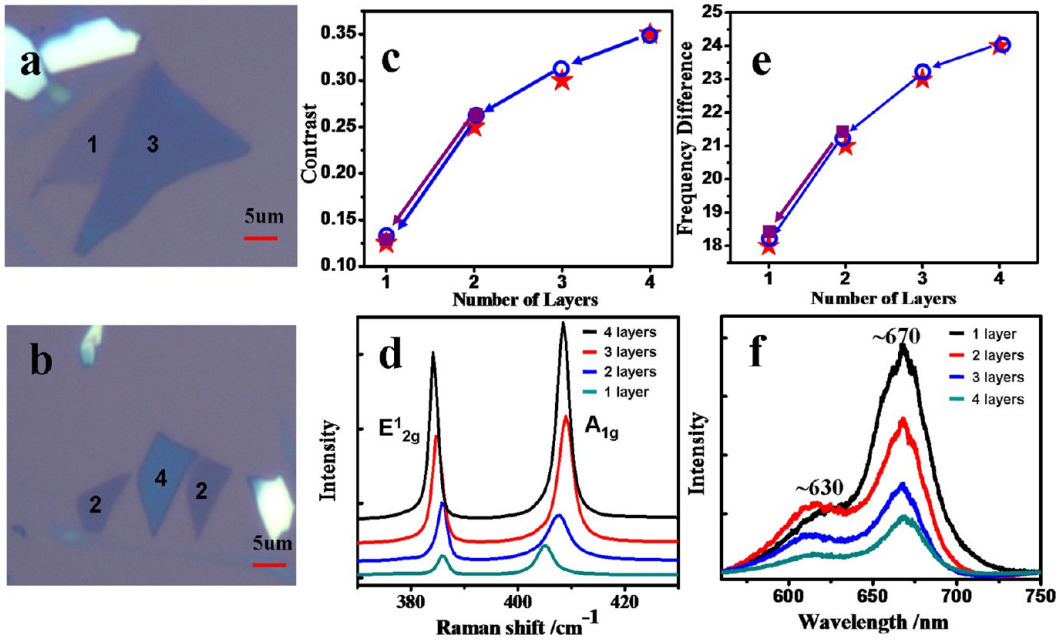

Figure 1. (a,b) Optical images of 1−4 layer MoS_2. (c) Contrast values of pristine 1−4 layer MoS_2 (red stars). Purple squares/blue circles represent the contrast values of a bilayer/quadrilayer MoS_2 sheet before and after plasma thinning. (d) Raman spectra of 1−4 layer MoS_2. (e) Frequency differences of E^1_{2g} and A_{1g} peaks of pristine 1−4 layer MoS_2 (red stars). Purple squares/blue circles represent the frequency differences of a bilayer/quadrilayer MoS_2 sheet before and after plasma thinning. (f) PL spectra of 1−4 layer MoS_2.

laser to thin MoS_2 sheets down to monolayer thickness.[30] However, the origin of laser thinning is thermal ablation which makes it only possible to produce single-layer MoS_2 and challenging for scale-up.[4,30] It would also be difficult to use this method to make high-resolution patterns (e.g., down to nanometer size), due to the optical diffraction limit of the laser spot.

Here, we present layer-by-layer thinning of multilayer MoS_2 down to the monolayer by using Ar^+ plasma. The thickness change is confirmed by atomic force microscopy (AFM), transmission electron microscopy (TEM), optical contrast, Raman, and PL spectra. The top layer MoS_2 is totally removed by plasma, while the bottom layer remains almost unaffected. We also demonstrate that, combined with standard lithographic techniques, this method can be used to prepare two-dimensional MoS_2 heterostructures with different thicknesses and sizes. A heterostructure composed of periodical single-layer and bilayer MoS_2 is presented. This method enables large-scale thickness control of MoS_2 and other two-dimensional materials.

RESULTS AND DISCUSSION

Figure 1a,b shows the optical images of MoS_2 sheets with a thickness of 1−4 layers. The optical contrast of MoS_2 increases with the increase of its thickness. In our previous work, we proposed to use the contrast between *R*/*G*/*B* values of the sample and substrate in an optical image to precisely determine the thickness of two-dimensional materials.[31] Here, the *R* channel contrast is used to determine the thickness of MoS_2 with the following equation:

$$C = \frac{R_{sub} - R_{sam}}{R_{sub}} \quad (1)$$

where *C* is the contrast of the MoS_2 sheet, R_{sub} and R_{sam} are the *R* channel values of the SiO_2/Si substrate and MoS_2 sheets obtained from the optical image. The contrast values for 1−4 layers of MoS_2 are 0.125, 0.25, 0.31, and 0.36 (red stars in Figure 1c), which agree quite well with the results obtained by Li *et al.* (*R* value differences between sample and substrate are 28, 56, and 72 for 1, 2, and 3 layers of MoS_2, respectively).[32] In our work, the use of contrast to determine the layer thickness is more quantitative as it does not depend on the intensity of incident light and parameters of the microscope. However, care should be taken when using contrast to determine the thickness of two-dimensional materials. The contrast value could be affected by the thickness of an oxide capping layer; for example, the contrast values of single-layer MoS_2 on 300 and 285 nm SiO_2/Si substrates are ~0.125 and ~0.11, respectively. The thickness of MoS_2 is further confirmed by Raman spectra. Raman spectroscopy has been widely used to study two-dimensional materials and to identify their thicknesses.[33−36] The Raman spectra of 1−4 layer MoS_2 are shown in Figure 1d. Two main Raman features are clearly presented, which correspond to E^1_{2g} (~385 cm^{-1}, in-plane vibration of two S atoms with respect to the Mo atom) and A_{1g} (~405 cm^{-1}, out-of-plane vibration of S atoms)

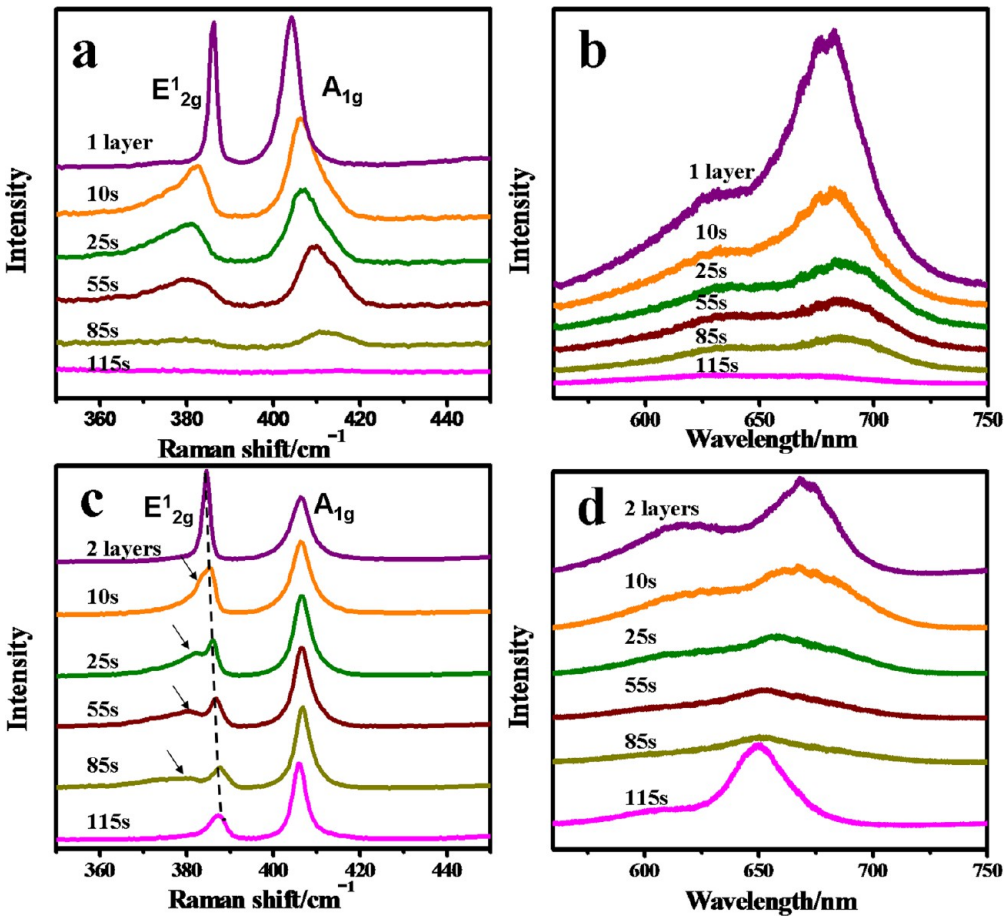

Figure 2. Raman (a) and PL (b) spectra of single-layer MoS_2 after Ar^+ plasma irradiation with different time. Raman (c) and PL (d) spectra of bilayer MoS_2 after plasma irradiation with different time.

modes.[35] The intensities of these two peaks increase with the increase of thickness. In addition, the frequency of the E^1_{2g} peak decreases and that of the A_{1g} peak increases with the increase of thickness, due to the change of force constant and also variation in the dielectric screening environment.[35,37] The frequency difference of these two peaks can then be used to identify the thickness of MoS_2 sheets. The red stars in Figure 1e show the frequency differences of E^1_{2g} and A_{1g} peaks, and the values are 18, 21, 23, and 24 cm^{-1} for 1−4 layer MoS_2, respectively. These results agree quite well with previous reports.[34−36] Figure 1f shows the PL spectra of 1−4 layer MoS_2. The PL spectra contain two peaks located at ~670 and ~630 nm, corresponding to the direct excitonic transitions between the minimum of the conduction band and the maxima of split valence bands (A1 and B1 excitons) in MoS_2.[9,10] The single-layer MoS_2 has a direct band gap structure; therefore, it has the strongest PL intensity. The PL intensity decreases with the increase of thickness.[10] The intensity difference between single-layer and multilayer MoS_2 is not as distinct as that reported by Mak *et al.*[9] but is similar to the result of Splendiani *et al.*[10] The PL intensity of single-layer MoS_2 can be greatly enhanced (by more than 10 times) after annealing in 300 °C in vacuum, while that of multilayer MoS_2 does not show noticeable changes. This might be the reason why different relative PL intensities of single-layer and multilayer MoS_2 were observed by different groups. The contrast values, Raman frequency differences, as well as PL intensities were used to monitor the thickness change of MoS_2 sheets after Ar^+ plasma irradiation.

Figure 2a,b shows Raman and PL spectra of single-layer MoS_2 after Ar^+ plasma irradiation (0−115 s). The Raman peaks become weak and broadened after plasma irradiation (10−85 s), which suggests that MoS_2 becomes disordered. After 115 s irradiation, the Raman peaks disappear, indicating that the single-layer MoS_2 is totally removed by plasma. The PL intensities of MoS_2 become much weaker with the increase of irradiation time (10−85 s), and it almost disappears after 115 s irradiation. The changes of Raman and PL spectra suggest that single-layer MoS_2 becomes disordered and can finally be removed by Ar^+ plasma. For bilayer MoS_2, the results are quite different. As can be seen in Figure 2c, the E^1_{2g} peak of bilayer MoS_2 splits after 10 s irradiation, as denoted by the black arrows. The emerging peak at ~380 cm^{-1} becomes broader and weaker (10−85 s) and finally

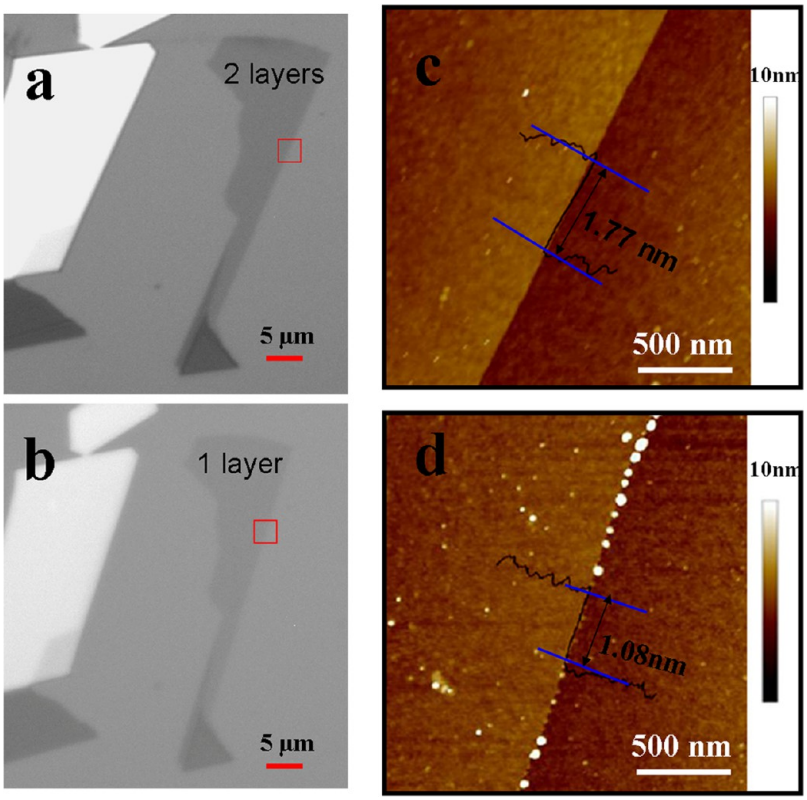

Figure 3. *R* channel optical images of a bilayer MoS_2 before (a) and after (b) Ar^+ plasma thinning. AFM images of the same sample before (c) and after (d) plasma thinning.

disappears (115 s) with the increase of irradiation time, similar to the E^1_{2g} peak of plasma-irradiated single-layer MoS_2 (Figure 2a). This suggests that the emerging peak belongs to the top layer MoS_2. Another interesting phenomenon is that, with the increase of irradiation time, the E^1_{2g} peak (the sharp peak belongs to the bottom layer) of bilayer MoS_2 shifts to higher frequency, toward the E^1_{2g} frequency of pristine single-layer MoS_2 (~385 cm^{-1}). It has been theoretically explained that the decrease of E^1_{2g} frequency with the increase of MoS_2 thickness is due to the stronger dielectric screening of the long-range Coulomb interaction in multilayer and bulk MoS_2.[37] The Ar^+ plasma irradiation introduces defects in the top layer MoS_2 and makes it disordered. As a result, the interlayer interaction between the top and bottom MoS_2 layers as well as the dielectric screening effect become much weaker, which results in the blue shift of E^1_{2g} peak after plasma irradiation. After 115 s irradiation, the E^1_{2g} and A_{1g} peaks of "bilayer" MoS_2 are very sharp and the frequency difference of these two peaks decreases from 21.5 cm^{-1} of bilayer MoS_2 to 18.5 cm^{-1}, which is the value of single-layer MoS_2 (purple squares in Figure 1e). In addition to Raman spectra, PL spectra of MoS_2 should give much clearer evidence of the thickness change, as the PL intensities of MoS_2 increase with the decrease of thickness.[9] As can be seen in Figure 2d, the PL intensities of bilayer MoS_2 decrease with the increase of irradiation time (10−85 s), as the top layer MoS_2 becomes disordered after plasma irradiation. After 115 s irradiation, the PL intensity has an abrupt increase, which is in agreement with the thickness change from bilayer to single-layer (indirect to direct band gap transition).

Figure 3a,b shows the *R* channel optical image of a bilayer MoS_2 before and after plasma thinning. The contrast values derived from these two images are 0.26 and 0.13 (purple squares in Figure 1c), respectively, close to the values of pristine bilayer and single-layer MoS_2. The AFM images are also presented in Figure 3c, d to study the morphologies of MoS_2 before and after plasma thinning. The thickness of pristine bilayer MoS_2 is ~1.77 nm, which is a bit larger than the theoretical value. This is a common observation for AFM images of layered materials, as there might be water or molecules trapped between the sample and substrate, and the trapping responses of the sample and substrate are also different.[36] The thickness of MoS_2 after plasma thinning is ~1.08 nm, with a thickness difference of ~0.69 nm compared to the pristine sample. This is quite close to the 0.62 nm interlayer spacing of bulk MoS_2.[38] It is worth noting that the surface of single-layer MoS_2 obtained by plasma thinning is still very smooth, with a roughness of 0.19 nm (0.18 and 0.13 nm for pristine single-layer and bilayer MoS_2), indicating that there are very few unremoved MoS_2 traces on the surface.[30]

High-resolution TEM is used to study the atomic structures of a bilayer MoS_2 before (Figure 4a−c) and

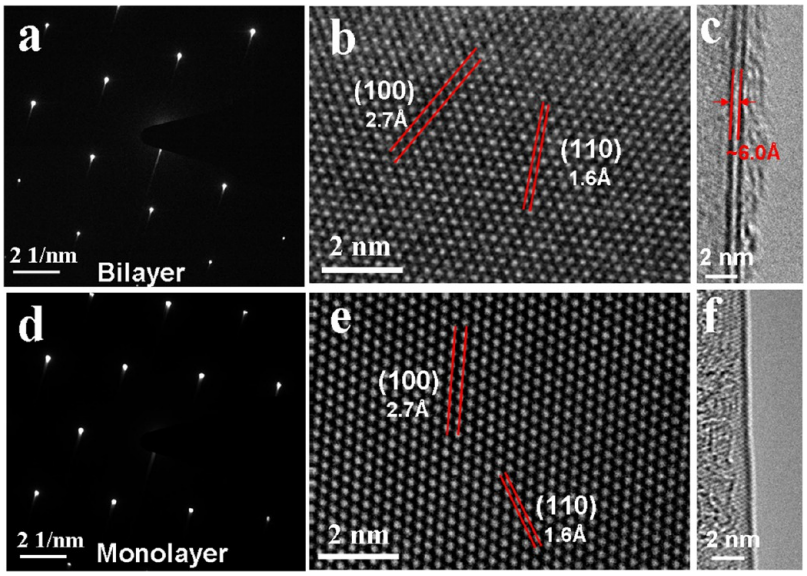

Figure 4. Diffraction patterns, high-resolution TEM images and folded edges of a pristine bilayer MoS_2 (a−c) and a plasma-thinned single-layer MoS_2 (d−f).

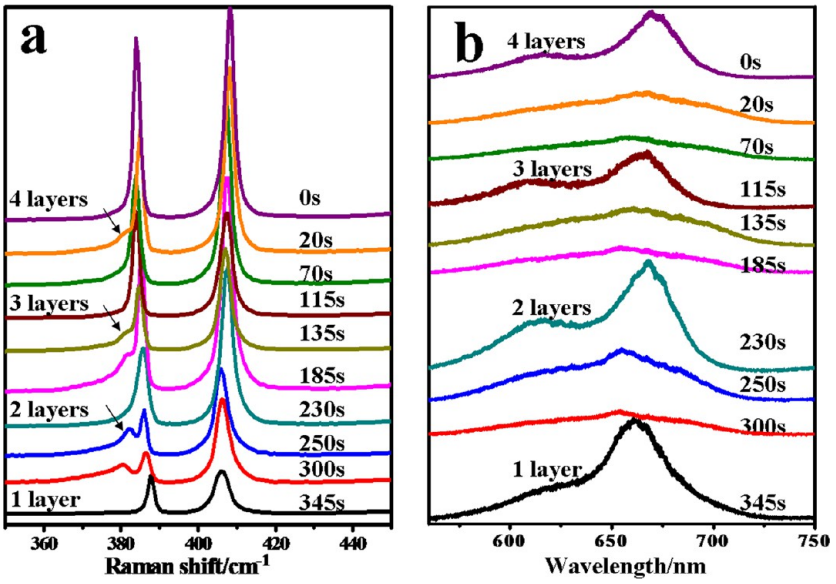

Figure 5. Raman (a) and PL (b) spectra of a the quadrilayer MoS_2 sheet after Ar^+ plasma irradiation with different time.

after (Figure 4d−f) plasma thinning. The electron diffraction patterns (Figure 4a,d) and high-resolution TEM images (Figure 4b,e) reveal the hexagonal lattice structure of MoS_2 with a lattice spacing of ~2.7 ((100) plane) and ~1.6 Å ((110) plane). No noticeable difference in the lattice parameters of MoS_2 is found before and after plasma thinning within the resolution of the system. The folded edges of two-dimensional materials are frequently adopted to identify the number of layers in TEM.[18,26,33,39] Bilayer MoS_2 presents two dark fringes with a space of ~6.0 Å, in good agreement with the interlayer distance of MoS_2. On the other hand, plasma-thinned single-layer MoS_2 has only one dark fringe. The most important observation of high-resolution TEM is that the structure of plasma-thinned single-layer MoS_2 remains extremely high quality (Figure 4e), indicating that the top layer MoS_2 is totally removed while the bottom layer remains almost unaffected by plasma. This may relate to the strong bonding strength of the S−Mo−S structure and the weak interlayer interaction. Plasma irradiation was also used to thin down graphene sheets.[40−42] However, reactive sources such as H_2O_2[42] and hydrogen[40] were used, which induced excessive defects in graphene. High-temperature (900 °C) post-annealing in O_2 was also used to etch the disordered top layer.[41] The S−Mo−S bonding of MoS_2 is not as strong as that of C−C bonding of graphene,[14,15] which makes MoS_2 more easily removed by Ar^+ plasma. We would emphasize that the plasma thinning of MoS_2 is highly reproducible and has

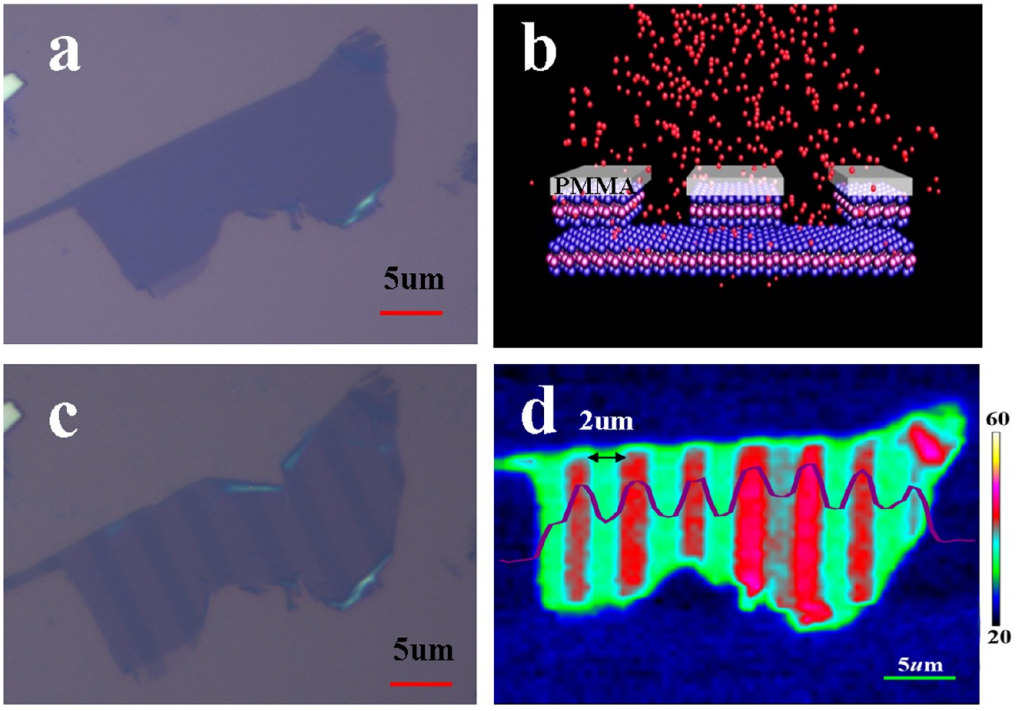

Figure 6. (a) Optical images of a pristine bilayer MoS_2. (b) Schematic showing the process of making the heterostructure. (c) Optical image of a periodical MoS_2 heterostructure obtained by plasma thinning. (d) Raman image generated by the intensities of the E^1_{2g} peak of the heterostructure. Inset is the cross section of the peak intensity across the sample.

almost 100% success rate for more than 10 processed samples. An important sign of thickness change is the abrupt increase of PL intensity after irradiation.

We can also do layer-by-layer thinning of MoS_2, as shown in Figure 5. A quadrilayer MoS_2 is irradiated by Ar^+ plasma with similar conditions (0−345 s). The E^1_{2g} peak first splits (as indicated by the black arrows in Figure 5a), and then the emerging peak disappears after 115 s irradiation. At the same time, the PL intensity has an abrupt increase (Figure 5b), indicating the removal of the topmost layer of MoS_2. Similar changes of Raman and PL spectra repeat for the removal of additional layers. The E^1_{2g} peak blue shifts, while the A_{1g} peak red shifts with the decrease of MoS_2 thickness. The frequency difference of E^1_{2g} and A_{1g} peaks changes from 24 cm^{-1} (quadrilayer) to 23.4 cm^{-1} (trilayers) to 21.5 cm^{-1} (bilayer) and, finally, to 18.2 cm^{-1} (single-layer) (as shown by the blue circles in Figure 1e). The *R* contrast value of MoS_2 decreases from 0.36 (quadrilayers) to 0.32 (trilayers) to 0.26 (bilayer) and, finally, to 0.125 (single-layer) (as shown by the blue circles in Figure 1c). These results suggest that the plasma thinning of MoS_2 is very reliable and can be used for devices which require structures with different thicknesses, such as phototransistors with thickness-modulated optical energy gaps. It can also be used to study the thickness-dependent properties of MoS_2 sheets. Moreover, this method can be easily scaled up for the wafer-size process. Combined with standard lithographic technique, it can also be used to fabricate continuous two-dimensional heterostructures.

As a demonstration, we fabricate a periodical 1/2/1/2/1...MoS_2 heterostructure. A pristine bilayer MoS_2 (Figure 6a) is spin-coated by a thin layer of polymethyl methacrylate (PMMA), followed by electron beam lithography to create a mask of periodical lines with a width of ~2 μm (Figure 6b). Ar^+ plasma is then used to thin down the uncovered area to form periodical heterostructures. The optical image of the obtained structure in Figure 6c shows MoS_2 patterns with different thicknesses/contrast. The Raman image created by the intensity of the E^1_{2g} peak is shown in Figure 6d. The red color represents higher Raman intensity (bilayer), and green color represents lower intensity (single-layer). Figure 6 demonstrates that, by using plasma irradiation and standard lithography, we can achieve arbitrary MoS_2 heterostructures with different thickness. The width of the structure can be at nanometer scale with careful control of experimental conditions. The periodical heterostructures containing materials with different electronic properties[43] (e.g., direct and indirect band gap structures for single-layer and bilayer MoS_2) may bring out interesting properties and new physics.

CONCLUSION

In summary, we have demonstrated that the thickness of MoS_2 sheets can be controlled layer-by-layer under Ar^+ plasma irradiation. AFM, high-resolution TEM, Raman, and PL spectra suggest that the top layer MoS_2 is totally removed, while the bottom layer MoS_2 remains almost unaffected, which makes this method

promising for fabricating electronic devices with different structures and thicknesses. We have also prepared a two-dimensional heterostructure containing periodical single-layer and bilayer MoS_2. The plasma thinning provides an easy and efficient way to control the properties of MoS_2 and other two-dimensional materials.

EXPERIMENTAL METHODS

Single-layer and multilayer MoS_2 are fabricated by mechanical exfoliation from single-crystal MoS_2 and deposited onto a 300 nm SiO_2/Si substrate. Optical microscopy, Raman, and AFM are used to identify the thickness. Ar^+ plasma (commercial 13.56 MHz RF source) with power of 50 W and pressure of 40 Pa is used to thin down the MoS_2 sheets with different irradiation time at room temperature. The Raman and PL spectra are recorded using a LabRAM HR800 Raman system with 514.5 nm excitation. The laser power at the sample is lower than 0.5 mW to avoid laser-induced heating. To obtain the Raman images, an $x-y$ stage is used to move the sample with a step size of 200 nm, and a Raman spectrum is recorded at every point. AFM is carried out with a Nanoscape 8.15 system. High-resolution TEM is carried out using an image aberration-corrected TEM system (FEI Titan 80-300). An acceleration voltage of 80 kV is chosen to achieve enough resolution while maintaining the structure of MoS_2. The MoS_2 flakes are transferred to a TEM grid using a PMMA-based transfer technique.[44] A thin layer of PMMA is spin-coated on the SiO_2/Si substrate which contains a target flake. The SiO_2 is etched away by KOH solution. The MoS_2 flake will attach on PMMA and will then be transferred to the TEM grid. An optical microscope is used to locate the flake and make aligned transfer. Finally, PMMA is dissolved in acetone, and the sample is washed by isopropyl alcohol and water several times.

Conflict of Interest: The authors declare no competing financial interest.

Acknowledgment. This work is supported by NSFC (11104026), Program for New Century Excellent Talents in University (NCET-11-0094), the 973 Programs (2011CB707601, 2009CB623702), Chinese postdoctoral fundings (No. 2012M520053), and Natural Science Foundation of Jiangsu Province (BK2011585, BE2011159).

REFERENCES AND NOTES

1. Novoselov, K. S.; Geim, A. K.; Morozov, S. V.; Jiang, D.; Zhang, Y.; Dubonos, S. V.; Grigorieva, I. V.; Firsov, A. A. Electric Field Effect in Atomically Thin Carbon Films. *Science* **2004**, *306*, 666.
2. Novoselov, K. S.; Jiang, D.; Schedin, F.; Booth, T. J.; Khotkevich, V. V.; Morozov, S. V.; Geim, A. K. Two-Dimensional Atomic Crystals. *Proc. Natl. Acad. Sci. U.S.A.* **2005**, *102*, 10451.
3. Pacilé, D.; Meyer, J. C.; Girit, Ç. Ö.; Zettl, A. The Two-Dimensional Phase of Boron Nitride: Few-Atomic-Layer Sheets and Suspended Membranes. *Appl. Phys. Lett.* **2008**, *92*, 133107.
4. Wang, Q. H.; Kalantar-Zadeh, K.; Kis, A.; Coleman, J. N.; Strano, M. S. Electronics and Optoelectronics of Two-Dimensional Transition Metal Dichalcogenides. *Nat. Nanotechnol.* **2012**, *7*, 699.
5. Roxlo, C. B.; Chianeili, R. R.; Deckman, H. W.; Ruppert, A. F.; Wong, P. P. Bulk and Surface Optical Absorption in Molybdenum Disulfide. *J. Vac. Sci. Technol.* **1987**, *5*, 555.
6. Radisavljevic, B.; Radenovic, A.; Brivio, J.; Giacometti, V.; Kis, A. Single-Layer MoS_2 Transistors. *Nat. Nanotechnol.* **2011**, *6*, 147.
7. Kim, S.; Konar, A.; Hwang, W. S.; Lee, J. H.; Lee, J.; Yang, J.; Jung, C.; Kim, H.; Yoo, J. B.; Choi, J. Y.; *et al.* High-Mobility and Low-Power Thin-Film Transistors Based on Multilayer MoS_2 Crystals. *Nat. Commun.* **2012**, *3*, 1011.
8. Liu, H.; Neal, A. T.; Ye, P. D. Channel Length Scaling of MoS_2 MOSFETs. *ACS Nano* **2012**, *6*, 8563.
9. Mak, K. F.; Lee, C.; Hone, J.; Shan, J.; Heinz, T. F. Atomically Thin MoS_2: A New Direct-Gap Semiconductor. *Phys. Rev. Lett.* **2010**, *105*, 136805.
10. Splendiani, A.; Sun, L.; Zhang, Y. B.; Li, T. S.; Kim, J.; Chim, C. Y.; Galli, G.; Wang, F. Emerging Photoluminescence in Monolayer MoS_2. *Nano Lett.* **2010**, *10*, 1271.
11. Mak, K. F.; He, K.; Shan, J.; Heinz, T. F. Control of Valley Polarization in Monolayer MoS_2 by Optical Helicity. *Nat. Nanotechnol.* **2012**, *7*, 494.
12. Zeng, H. L.; Dai, J. F.; Yao, W.; Xiao, D.; Cui, X. D. Valley Polarization in MoS_2 Monolayers by Optical Pumping. *Nat. Nanotechnol.* **2012**, *7*, 490.
13. Cao, T.; Wang, G.; Han, W. P.; Ye, H. Q.; Zhu, C. R.; Shi, J. R.; Niu, Q.; Tan, P. H.; Wang, E.; Liu, B. L.; *et al.* Valley-Selective Circular Dichroism of Monolayer Molybdenum Disulphide. *Nat. Commun.* **2012**, *3*, 887.
14. Castellanos-Gomez, A.; Poot, M.; Steele, G. A.; Van der Zant, H. S. J.; Agraït, N.; Rubio-Bollinger, G. Elastic Properties of Freely Suspended MoS_2 Nanosheets. *Adv. Mater.* **2012**, *24*, 772.
15. Bertolazzi, S.; Brivio, J.; Kis, A. Stretching and Breaking of Ultrathin MoS_2. *ACS Nano* **2011**, *5*, 9703.
16. Feng, J.; Qian, X. F; Huang, C. W.; Li, J. Strain-Engineered Artificial Atom as a Broad-Spectrum Solar Energy Funnel. *Nat. Photonics* **2012**, *6*, 866.
17. Lee, Y. H.; Zhang, X. Q.; Zhang, W. J.; Chang, M. T.; Lin, C. T.; Chang, K. D.; Yu, Y. C.; Wang, J. T.; Chang, C. S.; Li, L. J.; *et al.* Synthesis of Large-Area MoS_2 Atomic Layers with Chemical Vapor Deposition. *Adv. Mater.* **2012**, *24*, 2320.
18. Zhan, Y. J.; Liu, Z.; Najmaei, S.; Ajayan, P. M.; Lou, J. Large-Area Vapor-Phase Growth and Characterization of MoS_2 Atomic Layers on a SiO_2 Substrate. *Small* **2012**, *8*, 966.
19. Liu, K. K.; Zhang, W. J.; Lee, Y. H.; Lin, Y. C.; Chang, M. T.; Su, C. Y.; Chang, C. S.; Li, H.; Shi, Y. M.; Zhang, H.; *et al.* Growth of Large-Area and Highly Crystalline MoS_2 Thin Layers on Insulating Substrates. *Nano Lett.* **2012**, *12*, 1538.
20. Eda, G.; Yamaguchi, H.; Voiry, D.; Fujita, T.; Chen, M. W.; Chhowalla, M. Photoluminescence from Chemically Exfoliated MoS_2. *Nano Lett.* **2011**, *11*, 5111.
21. Smith, R. J.; King, P. J.; Lotya, M.; Wirtz, C.; Khan, U.; De, S.; O'Neill, A.; Duesberg, G. S.; Grunlan, J. C.; Moriarty, G.; *et al.* Large-Scale Exfoliation of Inorganic Layered Compounds in Aqueous Surfactant Solutions. *Adv. Mater.* **2011**, *23*, 3944.
22. Castro Neto, A. H.; Guinea, F.; Peres, N. M. R.; Novoselov, K. S.; Geim, A. K. The Electronic Properties of Graphene. *Rev. Mod. Phys.* **2009**, *81*, 109.
23. Yin, Z. Y.; Li, H.; Li, H.; Jiang, L.; Shi, Y. M.; Sun, Y. H.; Lu, G.; Zhang, Q.; Chen, X. D.; Zhang, H. Single-Layer MoS_2 Phototransistors. *ACS Nano* **2012**, *6*, 74.
24. Lee, H. S.; Min, S. W.; Chang, Y. G.; Park, M. K.; Nam, T.; Kim, H. J.; Kim, J. H.; Ryu, S.; Im, S. MoS_2 Nanosheet Phototransistors with Thickness-Modulated Optical Energy Gap. *Nano Lett.* **2012**, *12*, 3695.
25. Carladous, A.; Coratger, R.; Ajustron, F.; Seine, G.; Péchou, R.; Beauvillain, J. Light Emission from Spectral Analysis of Au/MoS_2 Nanocontacts Stimulated by Scanning Tunneling Microscopy. *Phys. Rev. B* **2002**, *66*, 045401.
26. Zhang, Y. B.; Tang, T. T.; Girit, C.; Hao, Z.; Martin, M. C.; Zettl, A.; Crommie, M. F.; Shen, Y. R.; Wang, F. Direct Observation of a Widely Tunable Bandgap in Bilayer Graphene. *Nature* **2009**, *459*, 820.
27. Thiti, T.; Kenji, W.; Takashi, T. C.; Pablo, J. H. Quantum Hall Effect and Landau-Level Crossing of Dirac Fermions in Trilayer Graphene. *Nat. Phys.* **2011**, *7*, 621.
28. Wang, H.; Yu, L.; Lee, Y. H.; Shi, Y.; Hsu, A.; Chin, M. L.; Li, L. J.; Dubey, M.; Kong, J.; Palacios, T. Integrated Circuits Based on Bilayer MoS_2 Transistors. *Nano Lett.* **2012**, *12*, 4674.
29. Choi, W.; Cho, M. Y.; Konar, A.; Lee, J. H.; Cha, G. B.; Hong, S. C.; Kim, S.; Kim, J. Y.; Jena, D.; Joo, J.; *et al.* High-Detectivity

Multilayer MoS_2 Phototransistors with Spectral Response from Ultraviolet to Infrared. *Adv. Mater.* **2012**, *24*, 5832.
30. Castellanos-Gomez, A.; Barkelid, M.; Goossens, A. M.; Calado, V. E.; Van der Zant, H. S. J.; Steele, G. A. Laser-Thinning of MoS_2: On Demand Generation of a Single-Layer Semiconductor. *Nano Lett.* **2012**, *12*, 3187.
31. Wang, Y. Y.; Gao, R. X.; Ni, Z. H.; He, H.; Guo, S. P.; Yang, H. P.; Cong, C. X.; Yu, T. Thickness Identification of Two-Dimensional Materials by Optical Image. *Nanotechnology* **2012**, *23*, 495713.
32. Li, H.; Lu, G.; Yin, Z. Y.; He, Q. Y.; Li, H.; Zhang, Q.; Zhang, H. Optical Identification of Single- and Few-Layer MoS_2 Sheets. *Small* **2012**, *8*, 682.
33. Ferrari, A. C.; Meyer, J. C.; Scardaci, V.; Casiraghi, C.; Lazzeri, M.; Mauri, F.; Piscanec, S.; Jiang, D.; Novoselov, K. S.; Roth, S.; *et al.* Raman Spectrum of Graphene and Graphene Layers. *Phys. Rev. Lett.* **2006**, *97*, 187401.
34. Li, H.; Zhang, Q.; Yap, C. C. R.; Tay, B. K.; Edwin, T. H. T.; Olivier, A.; Baillargeat, D. Q. From Bulk to Monolayer MoS_2: Evolution of Raman Scattering. *Adv. Funct. Mater.* **2012**, *22*, 1385.
35. Lee, C.; Yan, H.; Brus, L. E.; Heinz, T. F.; Hone, J.; Ryu, S. Anomalous Lattice Vibrations of Single- and Few-Layer MoS_2. *ACS Nano* **2010**, *4*, 2695.
36. Li, S. L.; Miyazaki, H.; Song, H. S.; Kuramochi, H.; Nakaharai, S.; Tsukagoshi, K. Quantitative Raman Spectrum and Reliable Thickness Identification for Atomic Layers on Insulating Substrates. *ACS Nano* **2012**, *6*, 7381.
37. Molina-Sanchez, A.; Wirtz, L. Phonons in Single-Layer and Few-Layer MoS_2 and WS_2. *Phys. Rev. B* **2011**, *84*, 155413.
38. Wakabayashi, N.; Smith, H. G.; Nicklow, R. M. Lattice Dynamics of Hexagonal MoS_2 Studied by Neutron Scattering. *Phys. Rev. B* **1975**, *12*, 659.
39. Brivio, J.; Alexander, D. T. L.; Kis, A. Ripples and Layers in Ultrathin MoS_2 Membranes. *Nano Lett.* **2011**, *11*, 5148.
40. Hazra, K. S.; Rafiee, J.; Rafiee, M. A.; Mathur, A.; Roy, S. S.; McLauhglin, J.; Koratkar, N.; Misra, D. S. Thinning of Multilayer Graphene to Monolayer Graphene in a Plasma Enviroment. *Nanotechnology* **2011**, *22*, 025704.
41. Yang, X. C.; Tang, S. J.; Ding, G. Q.; Xie, X. M.; Jiang, M. H.; Huang, F. Q. Layer-by-Layer Thinning of Graphene by Plasma Irradiation and Post-annealing. *Nanotechnology* **2012**, *23*, 025704.
42. Zhao, G. X.; Shao, D. D.; Chen, C. L.; Wang, X. K. Synthesis of Few-Layered Graphene by H_2O_2 Plasma Etching of Graphite. *Appl. Phys. Lett.* **2011**, *98*, 183114.
43. Eda, G.; Fujita, T.; Yamaguchi, H.; Voiry, D.; Chen, M. W.; Chhowalla, M. Coherent Atomic and Electronic Heterostructures of Single-Layer MoS_2. *ACS Nano* **2012**, *6*, 7311.
44. Pan, W.; Xiao, J. L.; Zhu, J. W.; Yu, C. X.; Zhang, G.; Ni, Z. H.; Watanabe, K.; Taniguchi, T.; Shi, Y.; Wang, X. R. Biaxial Compressive Strain Engineering in Graphene/Boron Nitride Heterostructures. *Sci. Rep.* **2012**, *2*, 893.